Electronic Supplementary Information

Conformational isomerism controls collective flexibility in metal-organic framework DUT-8(Ni)

Petko St. Petkov,[1,2] Volodymyr Bon,[3] Claire L. Hobday,[4] Agnieszka B. Kuc,[2,5] Patrick Melix,[2,3] Stefan Kaskel,[3] Tina Düren,[4] Thomas Heine[2,3,5]

1. University of Sofia, Faculty of Chemistry and Pharmacy, 1126, Sofia, Bulgaria
2. Lehrstuhl für Theoretische Chemie komplexer Systeme, Wilhelm-Ostwald-Institut für Physikalische und Theoretische Chemie, Universität Leipzig, Linnéstr. 2, 04103 Leipzig, Germany
3. Technische Universität Dresden, Fakultät Mathematik und Naturwissenschaften, Fakultät Chemie und Lebensmittelchemie, Bergstraße 66, 01069 Dresden, Germany
4. Centre for Advanced Separations Engineering, Department of Chemical Engineering, University of Bath, Bath BA2 7AY, U.K.
5. Helmholtz-Zentrum Dresden-Rossendorf, Abteilung Ressourcenökologie, Forschungsstelle Leipzig, Permoserstr. 15, 04318 Leipzig, Germany

Table of Contents

1. Born-Oppenheimer MD and well-tempered metadynamics

The calculations of periodic models of DUT-8(Ni) MOF were carried out using the QUICKSTEP[1] module of CP2K[2] with a mixed Gaussian and plane waves basis sets.[3] Periodic boundary conditions were applied in all three dimensions. The PBE exchange-correlation functional was used[4] with Goedecker–Teter–Hutter (GTH) pseudopotentials[5] incorporating scalar-relativistic core corrections. The orbital transformation method[6] was employed for an efficient wavefunction optimization. QUICKSTEP, as with nearly all ab initio Density Functional Theory simulation packages, requires the use of a real-space (RS) integration grid to represent certain functions, such as the electron density and the product Gaussian functions. QUICKSTEP uses a multi-grid system for mapping the product Gaussians onto the RS grid(s), so that wide and smooth Gaussian functions are mapped onto a coarser grid than narrow and sharp Gaussians. The electron density is always mapped onto the finest grid. Choosing a fine enough integration grid for a calculation is crucial in obtaining meaningful and accurate results. According to the manual of the code[7] a value of 50 +/- 10 Ry is required for highly accurate results, or for simulations with a variable cell. In our calculations the REL_CUTOFF parameter was set to 60 Ry. Contracted Gaussian basis sets of DZVP quality were used with a grid cutoff of 300 Ry for the BOMD simulations and 360 for the geometry optimization.[8] With this setup for the grid cutoff, 70% of the Gaussian functions are spawned on the finest grid and only 2% on the coarsest. In all calculations Grimme's DFT-D3 dispersion correction was applied.[9] In our study, a substantial part of the

dispersion interaction is associated with the π/π stacking of the naphthalene linkers. Therefore, we choose the PBE-D3 functional as it reproduces the experimental unit cell parameters for naphthalene molecular crystal with very high accuracy.[10] Born-Oppenheimer molecular dynamic (BOMD) simulations were performed in a fully flexible cells within the NPT ensemble at 300 K, 1.0 bar, and the equations of motion were integrated with a time step of 1.0 fs. Temperature and pressure were controlled via Nose thermostat.[11] In order to open thermodynamically more stable conformer **B(cl)°** and the transformation of **A(op)** to **B(op)** a well-tempered metadynamics (WTMTD) simulations[12] were performed. This method allows us to focus the computational effort only on the physically relevant regions of the collective variable space. ΔT parameter during the WTMTD was set to 1500 K and the simulations were performed in the phase space of two collective variables. The two independent collective variables for opening of the stable closed conformer, **B(cl)°**, correspond to the distance between the alpha-C atoms in the **ndc** linker, denoted as R(C1-C2) and R(C3-C4) in the Figure 4. Since we are interested only in the process of **B(cl)°** to **B(op)** conversion, after the pore of the MOF reached the open state the WTMTD simulation was stopped and the free energy barrier was estimated. Another set of two independent collective variables was used to simulate the transformation of **A(op)** to **B(op)**. In this case, the collective variables were defined as a torsion angle along alpha-C – carbonyl-C bond in two neighbouring **ndc** linkers. Vibrational analysis of **B(cl)°** and **B(op)** isomers were done with finite difference method as it is implemented in CP2K code. Due to the relatively flat potential energy surface for the two conformers, the vibrational analysis show four imaginary modes for each conformer with highest value of 195 cm^{-1}. The highest imaginary modes in both conformers correspond mostly to dabco rotation around Ni-Ni axes in the meal paddle-wheel moiety. The energy barrier for dabco rotation around Ni-Ni axes in the metal paddle-wheel moiety is in range of RT at 300K because it was observed during the BOMD simulation. In the zero-point energy and vibrational entropy estimates the imaginary modes were excluded.

2. Simulated adsorption mechanism

Due to the disorder in the crystal structure of DUT-8 in the **dabco** ligand, the experimental crystal structures was optimized prior to the adsorption simulation, as a chemically sensible model is required. Those DFT calculations were carried out using the periodic plane-wave DFT program CASTEP (16.11).[13] dE_{tot}/dE_{cut} < 0.003 eV per atom was achieved. For all simulations sampling of the Brillouin zone was achieved using a Monkhorst–Pack (MP) grid[14] with parameters chosen to result in a separation between k-points of generally no more than 0.08 Å. A cut-off energy of 650 eV and a MP grid of 1x1x1 was chosen for each system, using the PBE[4] functional approximating exchange and correlation with an additional Tkatchenko & Scheffler (TS) dispersion correction[15] applied, to account for long range van der Waals interactions. All structures were optimised using the Broyden-Fletcher-Goldfarb-Shanno (BFGS) algorithm.[16] The structure was considered to be optimised when the energy per atom, maximum force, maximum stress, and maximum atomic displacement converged to the values of 0.02 meV/atom, 0.05 eV/Å, 0.1 GPa, and 0.002 Å, respectively.

Grand canonical Monte Carlo simulations of N_2 adsorption in DUT-8 polymorphs

N_2 Gas adsorption was simulated using grand canonical Monte Carlo (GCMC) simulations, implemented in the multipurpose code MuSiC.[17] The simulations were carried out using atomistic models of the optimised experimental crystal structures **A(op)$_{exp}$** and **B(op)$_{exp}$** and the structures from the WTMD simulations **A(op)$_{comp}$** and **B(op)$_{comp}$**, where their atoms were fixed in the optimised positions. At each pressure, $1x10^7$ Monte Carlo steps were performed where each step consists of either a random translation, insertion or deletion, and random rotation – all equally weighted. The first 40 % of the steps were used for equilibration and the remaining used to calculate the ensemble averages. Standard Lennard-Jones (LJ) potentials were used to model the dispersive interactions

between the framework and gases. The framework metal atoms were modelled via the UFF force field,[18] the organic linkers were modelled with the Dreiding force field.[19] The Trappe force field was used to model N_2.[20] Coulombic interactions were included and calculated using Wolf Coulombic summations which are much more efficient than Ewald summations.[21] Interactions beyond 18 Å were neglected. To calculate the gas-phase fugacity the Peng–Robinson equation of state was used.[22]

Simulated adsorption mechanism

The simulated nitrogen isotherms at 77 K *via* GCMC of both the experimental structures and predicted phases of DUT-8 show that all polymorphs give rise to similar Type IV isotherms (**Figure S2a**), further simulation details are described in the SI. Through analysis of the interaction energies and the average positions of guest molecules, a general trend of the mechanism of adsorption could be deduced. At low pressure (up to 0.008 mbar) there is one distinct N_2 site (site 1) within DUT-8(Ni) ranging between -13.5 and -10 kJ mol^{-1}. At higher pressures (~0.1 mbar), a second site emerges, with slightly lower interaction energy with the framework (between -10 kJ mol^{-1} and -6 $kJmol^{-1}$), this second site allows for N_2 percolation down the b-axis. A third weakly interacting site (site 3) is present within the centre of the pore, at even higher N_2 pressures. Closer inspection of the simulated isotherms shows a step at 100 mbar, which is attributed to the ordering within the pores. At 1 bar N_2 pressure, the N_2 positions have well defined and ordered sites, **Figure S10** shows the positions of these sites within the framework. There is definite hierarchy of the sites, with site 1 favouring positions close to the metal centre with an average N_2-Ni distance of 4.6(3) Å. This creates channels of site 1 (red) positions in each corner of the pore down the *b*-axis. Site 2 (grey) is also positioned in channels running down the *b*-axis sitting in between each site 1 position. Site 3 sits in the centre of the pore and is only present at higher pressures due to higher loadings of N_2 in DUT-8, at these higher loadings N_2-N_2 interactions become dominant and drive formation of a third site.

The N_2 uptake for the different phases differs from 617 $cm^3\ g^{-1}$ for $\mathbf{A(op)_{exp}}$, 597 $cm^3\ g^{-1}$ for $\mathbf{B(op)_{exp}}$, 545 $cm^3\ g^{-1}$ for $\mathbf{A(op)_{comp}}$ and 587 $cm^3\ g^{-1}$ for $\mathbf{B(op)_{comp}}$ (**Table S2**). These differences can be accounted for by assessing both the pore size distribution as well as the interaction energy profile between the MOF and N_2 sorbate (**Figure S2b**). For example, the experimental structures: $\mathbf{A(op)_{exp}}$ and $\mathbf{B(op)_{exp}}$ give similar adsorption energy profiles and differ to those of the simulated $\mathbf{A(op)_{comp}}$ and $\mathbf{B(op)_{comp}}$ structures. On average $\mathbf{A(op)_{exp}}$ and $\mathbf{B(op)_{exp}}$ have a higher density of stronger interactions (around 11.3 kJ mol^{-1}) compared to $\mathbf{A(op)_{comp}}$ and $\mathbf{B(op)_{comp}}$ (around 10.9 kJ mol^{-1}).

The heat of adsorption for each framework in N_2 was calculated at each loading up to its maximum. Despite the difference in N_2 loading and energy range of adsorption sites, the heat of adsorption for each polymorph was within error of each (**Table S1-CLH**), which further confirms that conformational isomerism is difficult to distinguish.

Pore size distribution

The geometric pore size distributions for all DUT-8 structures were calculated using Poreblazer.[23] Here the pore size corresponds to the diameter of the largest sphere that can fit into the pore without overlapping with any of the framework atoms. The accessible surface area was calculated using a nitrogen-sized probe molecule (σ_N = 3.681 Å).

The differences between the pore sizes was relatively small, due to the large structural similarty. In general the pore sizes group the polymorphs into two separate groups with $\mathbf{A(op)_{comp}}$ and $\mathbf{B(op)_{exp}}$ have similar pore sizes (9.75 Å and 9.95 Å, respectively) and $\mathbf{B(op)_{comp}}$ and $\mathbf{A(op)_{exp}}$ having similar pore sizes (10.40 Å and 10.30 Å, respectively).

3. Crystallographic details

The asymmetric unit of experimental structure **B(op)$_{exp}$** contains one Ni atom, one half of the naphthalene-2,6-dicarboxylate (ndc) linker and a quarter of the disordered dabco molecule (Fig. S8b). The paddle wheel units and ndc linkers are complemented by inversion centres, while dabco molecule is generated by combination of the inversion centre and mirror plane. The analysis of the coordination geometry of the paddle wheel unit shows different orientations of the ndc linkers along [001] direction (conformer **B(op)**), caused by the 2-fold rotation axis running along [010] direction, through the inversion centre of the paddle wheel. In contrast, **ndc** linkers along [010] direction are generated by mirror plane, running through the paddle wheel unit, perpendicular to the 2-fold rotation axis. In contrast, in the tetragonal structure symmetrically dependent 2,6-ndc linkers are generated by 4-fold rotation axis running along [001] direction and therefore only conformer **A(op)** is possible. The structure solved in *C*2/*m* corresponds to the conformer **B(op)** predicted to be most energetically favourable in terms of ΔE relative upon structural transformations.

4. Figures S1 – S8

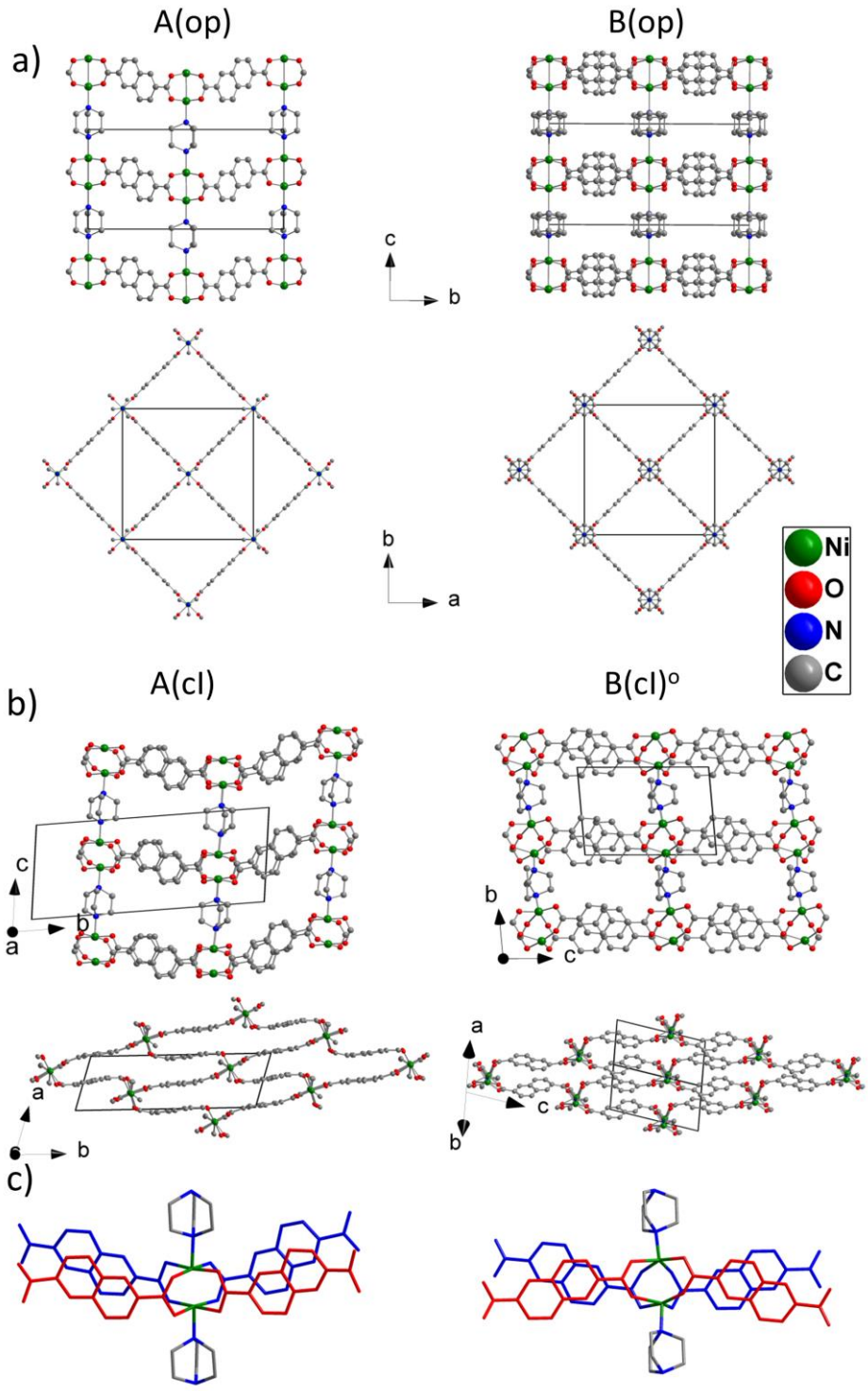

Figure S1. Atomistic structures representations of the DFT optimized conformer **A** and **B** in a) open forms, and b) closed forms. The stacking of the **ndc** linkers in the closed form of **A** and **B** is shown on panel (c).

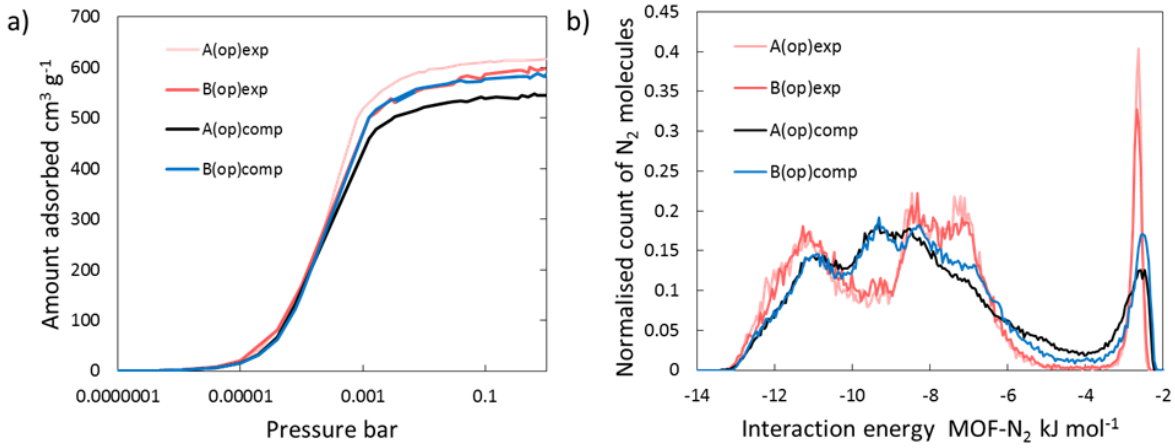

Figure S2. a) Simulated N_2 isotherms for DUT-8 polymorphs at 77 K. b) Interaction energy profile of MOF- N_2 energies for the different DUT-8 polymorphs at 1 bar and 77 K.

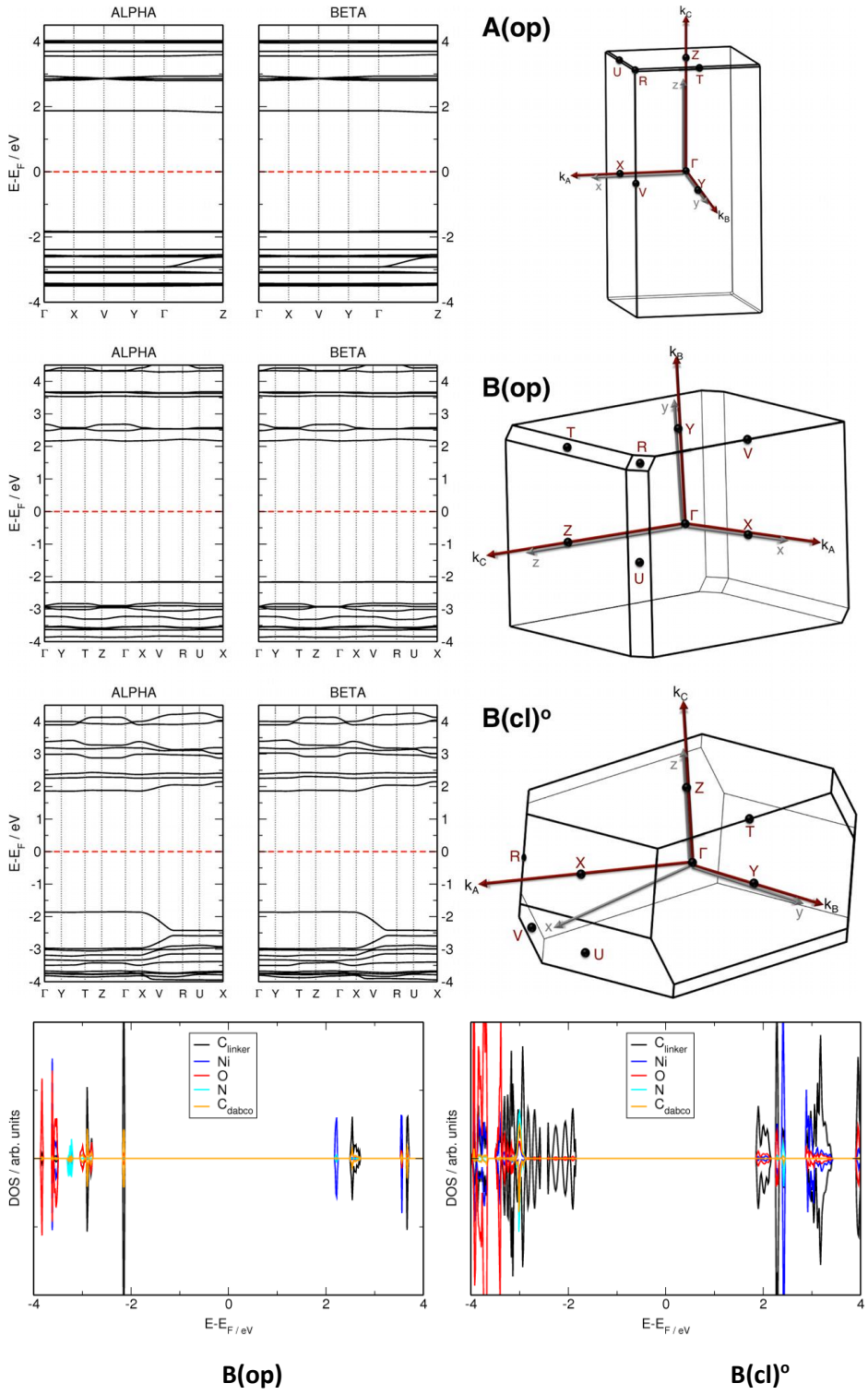

Figure S3. Calculated band structures (left) and the first Brillouin zones (right) of DUT-8(Ni) **A(op)** (top), **B(op)** (middle), and **B(cl)°** (bottom) forms. The Fermi level (horizontal dashed red lines) was shifted to zero. In the Brillouin zone representation, the red and gray arrows indicate the reciprocal (k_a, k_b, k_c) and real space (x, y, z) lattice vectors. Calculated PDOS for **B(op)** and **B(cl)°** are also shown. In the open form, the valence band maximum (VBM) is dominated by the C atoms from the linker and also a bit of C atoms from dabco. The conduction band minimum (CBM) is dominated by the two Ni atoms. Once closed, the VBM is nearly purely C atoms from the linkers, the same for the CMB. The

Ni states shift up in the energy. This is expectable, as in the closed form, there are strong interactions between the linkers.

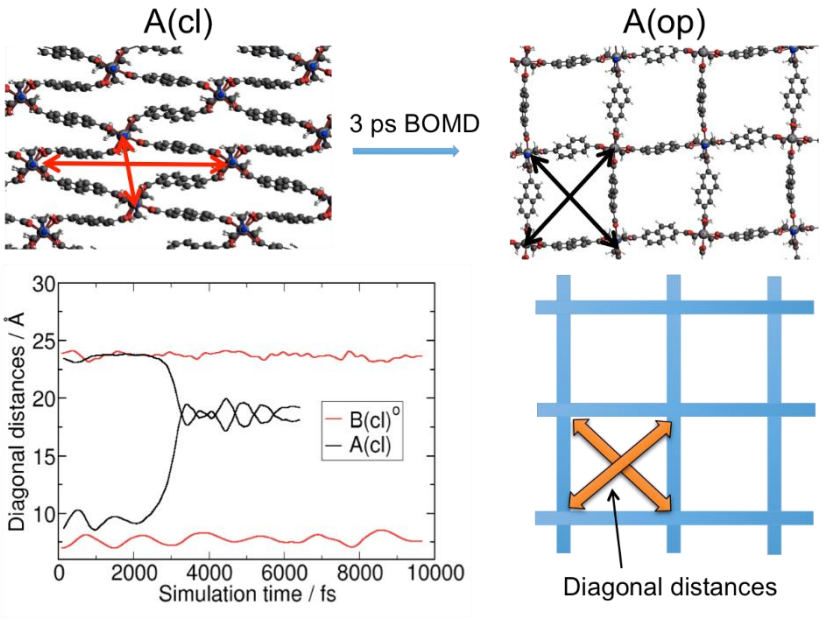

Figure S4. BOMD simulations of DUT-8(Ni) conformers **A** and **B**, starting from the corresponding closed forms. The pore size is monitored by the lengths of the pore diagonals as defined in the upper panel and the framework sketch.

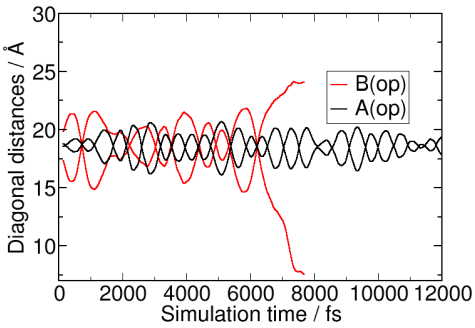

Figure S5. BOMD simulations of DUT-8(Ni) conformers **A** and **B**, starting from the corresponding open forms. Conventions as in Figure S4.

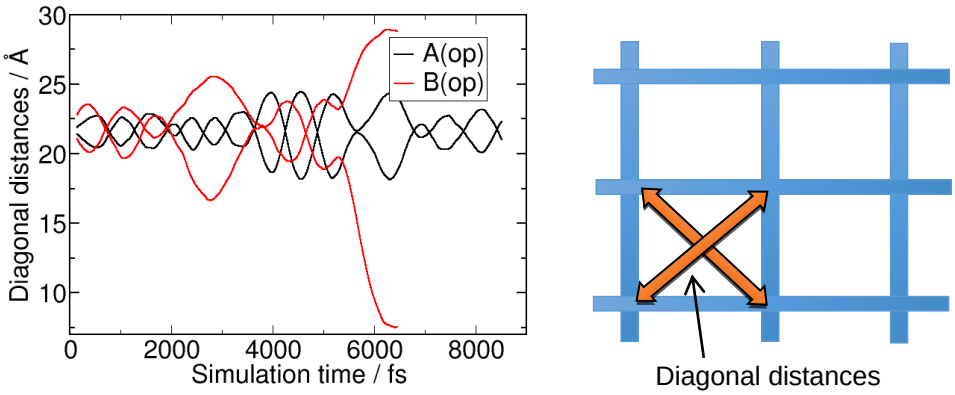

Figure S6. BOMD simulation of $Ni_2(adc)_2dabco$, the isotopological MOF to DUT-8(Ni) with anthracene dicarboxylic acid linkers, conformers **A** and **B**. Conventions are as in Figure S3.

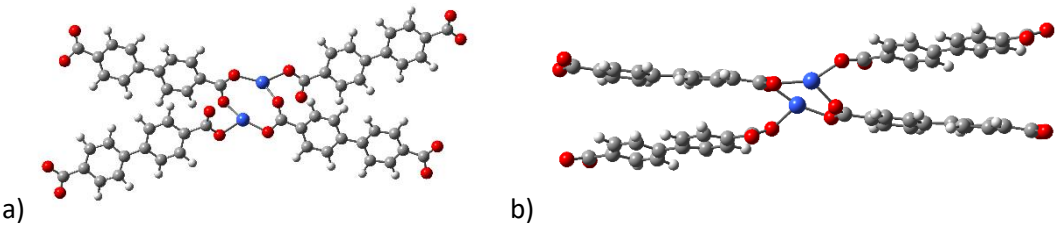

a) b)

Figure S7. Local structure of the closed form $Ni_2(bpdc)_2dabco$, the DUT-8(Ni) analogue with linear biphenyl dicarboxylate acid linkers. Distortion of in the Ni pw upon closure: (a) - side view and (b) - top view of the destroyed pw moiety.

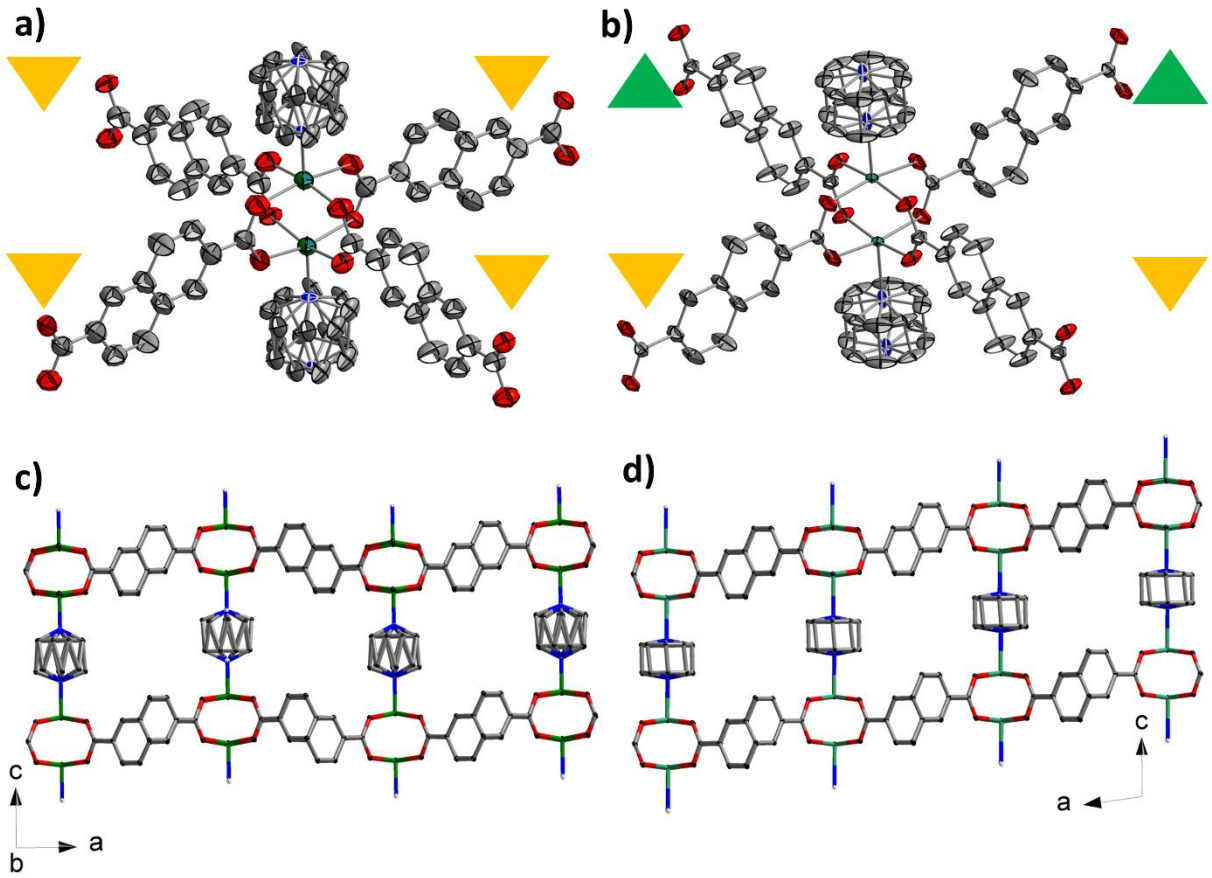

Figure S8. Crystal structure of DUT-8(Ni) conformers: a) local coordination geometry of the Ni-paddle-wheel in **A(op)**$_{exp}$; b) local coordination geometry of the Ni-paddle-wheel in **B(op)**$_{exp}$; c) parallel projection of **A(op)**$_{exp}$ structure along [010] direction; d) parallel projection of the crystal structure of **B(op)**$_{exp}$ along [010] direction.

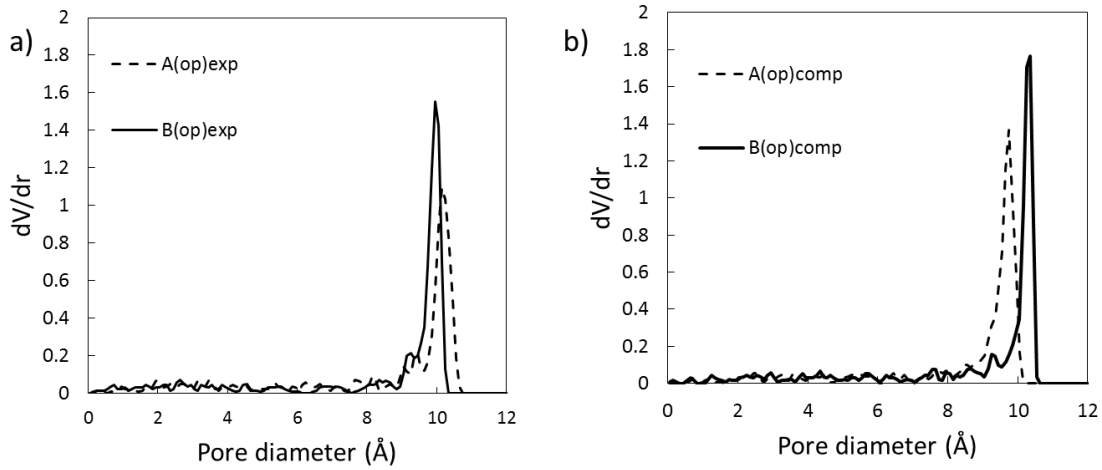

Figure S9. Calculated geometric pore size distribution of **A(op)** and **B(op)** experimental and theoretical structures

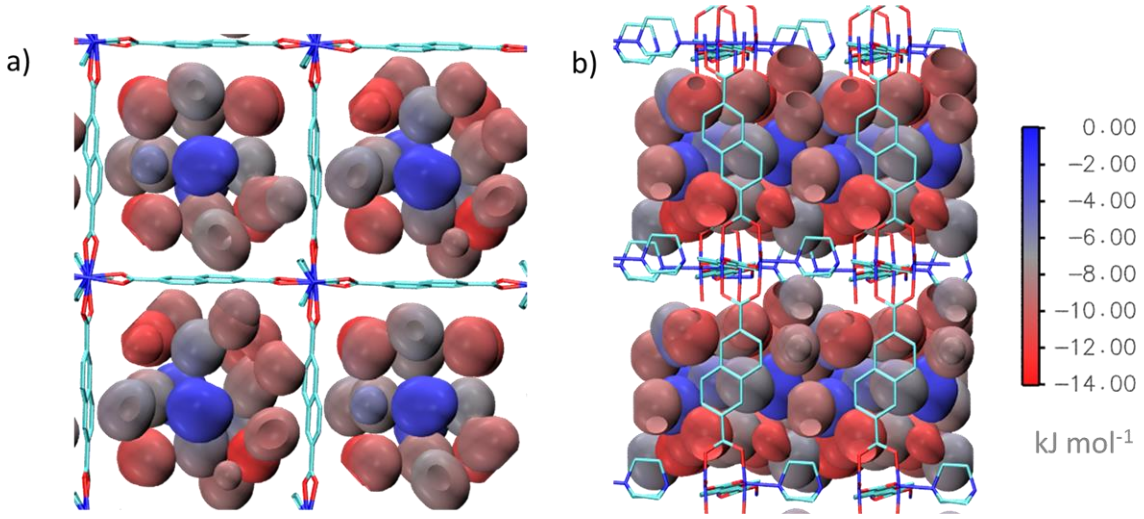

Figure S10. Representative density profiles of N_2 adsorption in DUT-8-op Surface shows the probability density of the N_2 adsorption site and the colour the respective energy of the site. Where red = -14 kJmol^{-1}-and blue = 0 kJ mol^{-1}

5. Tables S1 – S3

Table S1. Calculated cell parameters, cell vectors (in Å) and angles between the cell vectors (in °). Note that for conformer **A** the unit cell is twice larger (two Ni pw and four ndc linkers) than the unit cell for conformer **B** (one Ni pw and two ndc linkers).

	a	b	c	α	β	γ
A(op)	18.571	18.700	9.315	88.8	88.9	90.1
B(op)	18.621	18.477	9.552	90.6	90.1	94.1
A(cl)	8.153	23.492	9.319	85.3	103.6	83.2
B(cl)[a]	12.836	12.702	9.243	81.4	88.9	36.9
B(cl)[o]	7.106	7.772	12.364	89.6	105.08	102.5

Table S2. Single crystal X-ray diffraction data for tetragonal (conformer A) and monoclinic (conformer B) structures of DUT-8(Ni).

	DUT-8(Ni) A(op)$_{exp}$[24]	**DUT-8(Ni) B(op)$_{exp}$**
Empirical formula	C_{30} H_{24} N_2 Ni_2 O_8	C_{30} H_{24} N_2 Ni_2 O_8
Formula weight	657.91	657.93
***λ*, Å**	0.71073	0.71073
Crystal system, space group	tetragonal, *P4/n*	monoclinic, *C2/m*
Unit cell dimensions, Å	*a* = 18.4312(16) *c* = 9.3905(8)	*a* = 18.576(3) *b* = 18.408(2) *c* = 9.3574(13) β = 97.545(9)
Volume, Å^3	3190.0(5)	3172.0(7)
Z	2	2
***ρ*, g/cm^3**	0.685	0.689
***μ*, mm^{-1}**	0.614	0.618
F(000)	676	676
θ range, deg	2.2 – 30.8	2.2 – 26.9
Limiting indices	-26 ≤ h ≤ 26 -26 ≤ k ≤ 26 -11 ≤ l ≤ 13	-23 ≤ h ≤ 23 -23 ≤ k ≤ 22 -11 ≤ l ≤ 11
Reflections collected / unique	78281 / 4941	15439 / 3538
R(*int*)	0.269	0.0581
Data / parameters	11830 / 356	3538 / 127
GooF on F^2 [$I>2\sigma(I)$]	1.094 (after SQUEEZE)	1.151
Final *R* indices [$I>2\sigma(I)$], *R1, wR2*	0.1546, 0.3428 (after SQUEEZE)	0.0826, 0.2625
R* indices (all data), *R1, wR2	0.2418, 0.3858 (after SQUEEZE)	0.1029, 0.2809
Largest diff. peak / hole, *e*Å^{-3}	0.505 / -0.126 (after SQUEEZE)	1.64 / -2.33

Table S3: Structural data of DUT-8(Ni) conformational isomers.

DUT-8 polymorph	Q at low loading kJ mol^{-1}	Pore size (Å)	% porosity per unit cell	Simulated amount adsorbed $cm^3 g^{-1}$ (N_2, 1 bar, 77 K)
$A(op)_{exp}$	12.18	10.30	66.6	617
$B(op)_{exp}$	12.05	9.95	66.8	597
$A(op)_{comp}$	11.73	9.75	66.5	545
$B(op)_{comp}$	12.30	10.40	65.3	587

1 a) M. Krack and M. Parrinello, eds., *Quickstep. make the atoms dance*, NIC, Jülich, 2004; b) J. VandeVondele, M. Krack, F. Mohamed, M. Parrinello, T. Chassaing and J. Hutter, *Comp. Phys. Comm.*, 2005, **167**, 103;

2 CP2K 2017. www.cp2k.org, (accessed 28.03.20172017).

3 G. Lippert, J. Hutter and M. Parrinello, *Mol. Phys.*, 1997, **92**, 477.

4 J. P. Perdew, K. Burke and M. Ernzerhof, *Phys. Rev. Lett.*, 1996, **77**, 3865.

5 a) S. Goedecker, M. Teter and J. Hutter, *Phys. Rev. B*, 1996, **54**, 1703; b) C. Hartwigsen, S. Goedecker and J. Hutter, *Phys. Rev. B*, 1998, **58**, 3641; c) M. Krack, *Theor. Chem. Acc.*, 2005, **114**, 145;

6 J. VandeVondele and J. Hutter, *J. Chem. Phys.*, 2003, **118**, 4365.

7 CP2K Users Manual, https://manual.cp2k.org/trunk/CP2K_INPUT/FORCE_EVAL/DFT/MGRID.html#CUTOFF.

8 J. VandeVondele and J. Hutter, *J. Chem. Phys.*, 2007, **127**, 114105.

9 S. Grimme, J. Antony, S. Ehrlich and H. Krieg, *J. Chem. Phys.*, 2010, **132**, 154104.

10 J. Moellmann and S. Grimme, *J. Phys. Chem. C*, 2014, **118**, 7615.

11 G. Bussi, D. Donadio and M. Parrinello, *J. Chem. Phys.*, 2007, **126**.

12 a) M. Iannuzzi, A. Laio and M. Parrinello, *Phys. Rev. Lett.*, 2003, **90**; b) A. Laio and M. Parrinello, *Proc. Natl. Acad. Sci.*, 2002, **99**, 12562;

13 S. J. Clark, M. D. Segall, C. J. Pickard, P. J. Hasnip, M. I. J. Probert, K. Refson and M. C. Payne, *Z. Krist.*, 2005, **220**, 191.

14 H. J. Monkhorst and J. D. Pack, *Phys. Rev. B*, 1976, **13**, 5188.

15 A. Tkatchenko and M. Scheffler, *Phys. Rev. Lett.*, 2009, **102**, 73005.

16 D. F. Shanno, *Math. Comp.*, 1970, **24**, 647.

17 A. Gupta, S. Chempath, M. J. Sanborn, L. A. Clark and R. Q. Snurr, *Mol. Sim.*, 2003, **29**, 29.

18 A. K. Rappe, C. J. Casewit, K. S. Colwell, W. A. Goddard and W. M. Skiff, *J. Am. Chem. Soc.*, 1992, **114**, 10024.

19 S. L. Mayo, B. D. Olafson and W. A. Goddard, *J. Phys. Chem.*, 1990, **94**, 8897.

20 J. J. Potoff and J. I. Siepmann, *AIChE J.*, 2001, **47**, 1676.

21 D. Wolf, P. Keblinski, S. R. Phillpot and J. Eggebrecht, *J. Chem. Phys.*, 1999, **110**, 8254.

22 D.-Y. Peng and D. B. Robinson, *Ind. Eng. Chem. Fund.*, 1976, **15**, 59.

23 L. Sarkisov and A. Harrison, *Mol. Sim.*, 2011, **37**, 1248.

24 N. Klein, C. Herzog, M. Sabo, I. Senkovska, J. Getzschmann, S. Paasch, M. R. Lohe, E. Brunner and S. Kaskel, *Phys. Chem. Chem. Phys.*, 2010, **12**, 11778.